C Journal of Carbon Research

MDPI

Article

First-Principles Study of the Electronic Properties and Thermal Expansivity of a Hybrid 2D Carbon and Boron Nitride Material

Okikiola Olaniyan [1,*] and Lyudmila V. Moskaleva [1,2,*]

[1] Department of chemistry, University of the Free State, Bloemfontein 9300, South Africa
[2] Institute of Applied and Physical Chemistry and Center for Environmental Research and Sustainable Technology, University of Bremen, 28359 Bremen, Germany
* Correspondence: okikiola.olaniyan@gmail.com (O.O.); moskaleval@ufs.ac.za (L.V.M.)

Abstract: In an attempt to push the boundary of miniaturization, there has been a rising interest in two-dimensional (2D) semiconductors with superior electronic, mechanical, and thermal properties as alternatives for silicon-based devices. Due to their fascinating properties resulting from lowering dimensionality, hexagonal boron nitride (h-BN) and graphene are considered promising candidates to be used in the next generation of high-performance devices. However, neither h-BN nor graphene is a semiconductor due to a zero bandgap in the one case and a too large bandgap in the other case. Here, we demonstrate from first-principles calculations that a hybrid 2D material formed by cross-linking alternating chains of carbon and boron nitride (HCBN) shows promising characteristics combining the thermal merits of graphene and h-BN while possessing the electronic structure characteristic of a semiconductor. Our calculations demonstrate that the thermal properties of HCBN are comparable to those of h-BN and graphene (parent systems). HCBN is dynamically stable and has a bandgap of 2.43 eV. At low temperatures, it exhibits smaller thermal contraction than the parent systems. However, beyond room temperature, in contrast to the parent systems, it has a positive but finitely small linear-thermal expansion coefficient. The calculated isothermal bulk modulus indicates that at high temperatures, HCBN is less compressible, whereas at low temperatures it is more compressible relative to the parent systems. The results of our study are important for the rational design of a 2D semiconductor with good thermal properties.

Keywords: density functional perturbation theory (DFPT); linear thermal expansion coefficient; bulk modulus; hybrid material; graphene; hexagonal boron nitride (h-BN); specific heat capacity at constant pressure

Citation: Olaniyan, O.; Moskaleva, L.V. First-Principles Study of the Electronic Properties and Thermal Expansivity of a Hybrid 2D Carbon and Boron Nitride Material. *C* **2021**, *7*, 5. https://doi.org/10.3390/c7010005

Received: 16 December 2020
Accepted: 6 January 2021
Published: 12 January 2021

1. Introduction

Two-dimensional (2D) semiconductors with good thermal properties are at the forefront of nanoscience research as replacements for silicon-based devices. Graphene (sp^2 hybridized carbon atoms) and hexagonal boron nitride (h-BN) (sp^2 hybridized boron and nitrogen atoms) are considered as potential 2D materials for the next generation of electronics [1–4] due to their excellent electronic [5–9], mechanical [10,11], and thermal [12–15] properties. Despite the fascinating properties of these 2D materials, in pristine form they are not suitable for applications in devices in which semiconductors are required. This is because graphene is a zero-band-gap [16,17] material, while h-BN is an insulator with a large bandgap [16]. Due to these limitations, vigorous research is ongoing to explore the physical properties of other exciting 2D materials such as h-MoS_2 [8], h-$MoSe_2$ [18], borene [19], BC_3 [20,21], BC_5 [22], BC_7 [21], and recently h-BN-graphene hybrid [16,23,24], a layered material with regions of carbon and boron nitride.

Ever since the synthesis by Ci et al. [25], the h-BN-graphene hybrid has been the subject of intensive studies due to the unique, tailorable, and complementary properties to the h-BN and graphene. C, B, and N atoms can be mixed atomically together to form an

array of thermodynamically stable BCN layered materials with varying properties. For example, as a result of the similar lattice constants, h-BN and graphene can be synthesized as a layer-by-layer heterostructure [26–28]. Theoretical computations have revealed that a slight bandgap can be opened by depositing graphene on a h-BN substrate [29]. Another form of h-BN-graphene hybrid is an atomically thick material consisting of h-BN and graphene (2D-BNC) phases. This type of hybrid heterostructure is interesting because its physical properties can be tuned by varying the size of the domains and geometries of the h-BN domain with respect to the graphene or vice versa [23,24,30,31]. In one of our reports, we demonstrated the tunability of the thermodynamic and electronic properties of a 2D h-BN-graphene hybrid by changing the domain size of the h-BN [16]. In other studies, transport [32,33], magnetic [24], optical [34], and mechanical [35] properties have also been reported to be tunable by changing the concentration and shape of h-BN or graphene domains in the hybrid material. However, despite many reports on 2D-BNC, the linear thermal expansion coefficients (LTECs) of these materials, which is one of the fundamental quantities for heat management, have not been investigated.

Although reports on the LTEC of 2D-BNC are lacking, there is quite a number of studies on the LTEC of h-BN and graphene. All of them consistently indicate that h-BN and graphene both exhibit negative LTEC. Employing density functional perturbation theory (DFPT) within quasiharmonic approximation (QHA) [36], Mounet et al. [37] studied the LTEC of graphene at room temperature and observed that the value is approximately -3.6×10^{-6} K^{-1}. Moreover, they indicated that the LTEC of graphene remains negative even beyond 2000 K. In another study, Zakharchenko et al. [38,39], employing the Monte Carlo method with the empirical bond order potential [40], reported a slightly different average value of around -5.0×10^{-6} K^{-1} within the interval of 0 to 300 K and negative LTEC up to 900 K. Contrary to the theoretical estimates, an experimental investigation by Bao et al. [41] found negative LTEC only up to 350 K, and the value at room temperature was -7.0×10^{-6} K^{-1}. In another experimental study, in which the substrate effect was carefully excluded, Yoon et al. [42] measured the LTEC of graphene at 200–400 K and reported different results from the earlier reports. At variance to measurements of ref. [41], they found the LTEC to be negative in the whole temperature range. The LTEC of h-BN was estimated in a theoretical study by Sevik [18], using DFPT and QHA, in the temperature interval of 0 to 300 K as -6.6×10^{-6} K^{-1}.

As stated earlier, in contrast to h-BN and graphene, the LTECs of h-BN-graphene hybrids are lacking in the literature. However, the knowledge of the LTEC of the h-BN-graphene hybrid is important due to its potential application in ultra-fast integrated electronic devices. In this study, our aim was to characterize the LTEC of one type of h-BN-graphene hybrid, namely cross-linked alternating chains of carbon and boron nitride (HCBN). Currently, not much is known about HCBN, and to the best of our knowledge, the thermodynamic properties have not been reported elsewhere. For a comprehensive understanding of the material, other properties computationally predicted in this study were the electronic density of states, specific heat capacity at constant pressure, and isothermal bulk modulus. We also calculated the corresponding properties for h-BN and graphene in order to highlight how the properties of HCBN relate to the parent systems.

2. Computational Methods

VASP code [43,44] was employed to perform electronic structure calculations based on density functional theory (DFT). The projected augmented wave (PAW) method [45] was used to describe the interactions between the valence and core electrons. We applied the local density approximation (LDA) [46] and the generalized gradient approximation (GGA) [47] in the parameterization of Perdew, Burke, and Ernzerhof (PBE), for the exchange–correlation energy functional. While LDA was used for the phonon calculations, PBE was employed for structural optimization as well as to compute the density of states (DOS) of the two-dimensional systems in this study. It is worth mentioning that LDA and PBE fundamentally lower the bandgaps of semiconductors. In view of this, we applied

a hybrid functional (HSE06) [48] by Heyd–Scuseria–Ernzerhof to improve the result of the bandgap. The Brillouin zone (BZ) sampling was done using the Monkhorst–Pack scheme [49] and the $9 \times 7 \times 1$ k-point mesh for the total energy calculations, while denser k points of $21 \times 11 \times 1$ were employed to compute the density of states (DOS). The phonon dispersion relation was calculated along a sampling route that connects the unique symmetry points in the BZ as shown in Figure 1. We used 520 eV as the cutoff in the plane-wave expansion while treating fractional occupancies using the tetrahedron method with Blöchl corrections. The cohesive energy E_{coh} was calculated at the PBE level using Equation (1),

$$E_{coh} = \frac{-E_{CBN} + n_C E_C + n_B E_B + n_N E_N}{N_{at}} \quad (1)$$

where E_{CBN}, E_C, E_B, and E_N denote the total energies of HCBN, free C, B, and N atoms, respectively. The number of C, B, and N atoms present in the supercell are denoted by n_C, n_B, and n_N, respectively, while N_{at} is the total number of atoms in the supercell. Note that with this definition, the cohesive energy is a positive number.

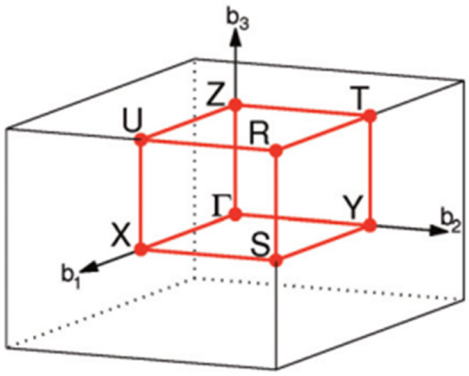

Figure 1. Brillouin zone sampling of orthorhombic lattice in the direction of Γ–*X*–*S*–*Y*–Γ–*Z*–*U*–*R*–*T*–*Z*|*Y*–*T*|*U*–*X*|*S*–*R*.

Lattice dynamics was calculated by the density functional perturbation theory (DFPT). Supercells with 50 atoms were used for h-BN and graphene, while the supercell of HCBN was composed of 48 atoms. The force constants were computed followed by the construction of a dynamical matrix. We obtained phonon frequencies through the diagonalization of the dynamical matrix. Thermal properties were calculated using quasiharmonic approximation (QHA) [50]. For a harmonic crystal, the Helmholtz free energy F is expressed as a sum of the ground-state energy and the vibrational free energy. The phonon contribution to the free energy is given by Equation (2):

$$F_{vib} = \frac{1}{2}\sum_{q,v} \hbar\omega_{q,v} + k_B T \sum_{q,v} \ln[1 - \exp(-\hbar\omega_{q,v}/(k_B T))] \quad (2)$$

where q and v represent the wave vector and the band index, respectively. $\omega_{q,v}$ denotes vibrational frequency at q and v. T, k_B, and $\hbar$ are the temperature, Boltzmann constant, and reduced Planck constant, respectively. The heat capacity C_v and the entropy S at constant volume were calculated using Equations (3) and (4), respectively:

$$C_v = \sum_{q,v} k_B \left(\frac{\hbar\omega_{q,v}}{k_B T}\right)^2 \frac{\exp\left(\frac{\hbar\omega_{q,v}}{k_B T}\right)}{\left[\exp\left(\frac{\hbar\omega_{q,v}}{k_B T}\right) - 1\right]^2} \quad (3)$$

and

$$S = -\frac{1}{T}\sum_{q,v} \frac{\hbar\omega_{q,v}}{\exp\left(\frac{\hbar\omega_{q,v}}{k_B T}\right) - 1} - k_B \sum_{q,v} \ln[1 - \exp(-\hbar\omega_{q,v}/(k_B T))] \quad (4)$$

We computed the heat capacity at constant pressure C_p using Equation (5),

$$C_p = -\frac{T\partial^2 G(T,p)}{\partial T^2} = \frac{T\partial V(T,p)}{\partial T}\frac{\partial S(T;V)}{\partial V} + C_V[T, V(T,P)] \quad (5)$$

where Gibbs free energy, G, is given by

$$G(T,p) = \min_V [U(V) + F_{vib}(T;V) + PV] \quad (6)$$

and V is the equilibrium volume at T and p. To calculate the thermodynamic properties at constant pressure, $U(V)$ and F_{vib} were computed at 10 volume points, and Equation (6) was fitted to the Birch-Murnaghan equation of state. The temperature-dependent LTEC ($\alpha(T)$) was calculated using Equation (7)

$$\alpha(T) = \frac{\partial \ln a(T)}{\partial T} = \frac{1\partial V}{2V\partial T} \quad (7)$$

where $a(T)$ represents the lattice parameter which corresponds to the minimum Gibbs free energy at a given temperature, while other parameters maintain their previous designations. To compute Equation (7), we kept the vacuum spacing at 15 Å and varied the in-plane lattice constant within $\pm 0.5\%$ for 10 different volumes of the slab. It is important to maintain small applied strain, typically within $\pm 0.5\%$, otherwise QHA becomes invalid. It is worth stating that the contribution of electronic thermal excitation energy to the thermal properties can be neglected in any material if the bandgap is greater than the excitation energy. However, in metallic systems, such contribution must be accounted for, since metals lack a bandgap and have non-zero electron density at the Fermi level. In the case of graphene, although it is a semimetal, the electronic structure is different from other metals. The bandgap only vanishes at the Dirac point where the electronic density is zero [17,51]. Consequently, the contribution of electronic excitation can be neglected in this material, and the thermal occupation of the phonon modes can be used to account for the thermal properties.

3. Results and Discussion

3.1. Structural Model and Electronic Properties

A two-dimensional hybrid with alternating chains of carbon and boron nitride (HCBN) is shown in Figure 2. The system has a rectangular lattice (as indicated by a rectangular dashed frame in Figure 2) with two carbon atoms, one boron, and one nitrogen atom per primitive cell. The optimized in-plane lattice parameters of the hybrid system, calculated at the PBE level, are a = 2.51 Å and b = 4.35 Å. We compared the predicted lattice parameters with that of the lattice constant of h-BN. Our predicted "a" is the same as the lattice constant of h-BN, while "b" is a factor of 1.7 larger. Meanwhile, our calculation shows that the lattice constant of h-BN is 2.51 Å, which agrees with the existing data from other studies [18]. The coordination of every atom in the primitive cell of HCBN was analyzed. It was observed that every C atom is bonded to two other C atoms and either a N or B atom, while every N (or B) atom is connected to two B (or N) atoms.

C-C and B-N bond lengths of the HCBN were computed and compared with the values for pristine graphene and h-BN, respectively. Our calculated C-C bond length of graphene was 1.43 Å, which was the same as the C-C bond length in HCBN. However, in the case of h-BN, we obtained the B-N bond length of 1.45 Å, which was slightly shorter than the corresponding bond distance in HCBN, 1.46 Å. Furthermore, we computed C-B and C-N bond lengths of 1.52 and 1.39 Å, respectively. Due to a slight difference between C-C and B-N, and a significant difference between C-B and C-N, there could be intrinsic structural stress in HCBN, which might affect the stability.

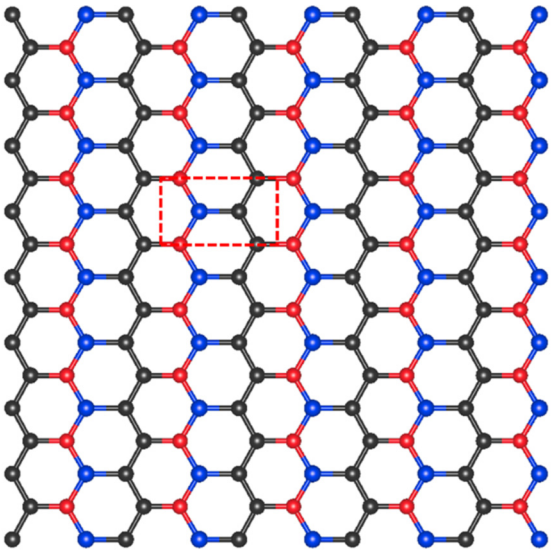

Figure 2. Atomic structure of carbon and boron nitride hybrid (HCBN) with alternating chains optimized at the Perdew, Burke, and Ernzerhof (PBE) level. The black, blue, and red spheres represent carbon, boron, and nitrogen atoms, respectively.

To assess the relative stability of HCBN, we calculated its cohesive energy and compared it with that of graphene and h-BN using Equation (1). The calculated cohesive energy of HCBN is 7.25 eV/atom, which is greater than 7.06 eV/atom for h-BN but less than 7.90 eV/atom for graphene. Thus, the cohesive energy indicates that HCBN is very stable with respect to the parent systems.

To analyze the electronic characteristics of HCBN accurately, we computed the total density of states (DOS) and partial density of states (PDOS) using PBE and HSE06 functionals as shown in Figure 3. From the DOS results, it is seen that HCBN is a semiconductor with a finite bandgap. With the PBE functional, we obtained a bandgap of 1.83 eV (Figure 3a). It is widely known that PBE underestimates the bandgap of semiconductors. To get an improved result, we applied the HSE06 functional, which is known to give reliable results for bandgaps of semiconductors, and obtained a bandgap of 2.43 eV (Figure 3b). The calculated bandgap shows that HCBN has a different electronic structure with respect to graphene and h-BN; while the former is a semimetal, the latter is an insulator with a bandgap of approximately 6.0 eV [16,52]. To understand the origin of the bandgap, the states around it were analyzed using the PDOS of Figure 3a. The valence band maximum (VBM) and the conduction band minimum (CBM) are formed by the mixing of the C and N 2p orbitals. Moreover, it is important to emphasize that the states around the VBM are dominated by C atoms while CBM originates predominantly from N atoms.

It is important to suggest how HCBN can be synthesized, since we have demonstrated that the system is thermodynamically stable. To synthesize HCBN, we expect a thermal catalytic chemical vapor deposition (CVD) technique, which is promising for large-area growth of graphene [53], to be applicable. An ideal substrate to use for the deposition would be Cu, since it has previously been successfully employed for both graphene [54] and h-BN [55] deposition. Graphene growth on a Cu substrate has been proposed to take place through a surface-adsorption mechanism [56]. The implication of this is that it might be possible to deposit HCBN on Cu by simultaneously annealing C and BN (such as BCl_3 and CH_3CN) containing precursors in the CVD. The ratio of B, N, and C in the hybrid can then be controlled by varying the thermodynamic growth conditions.

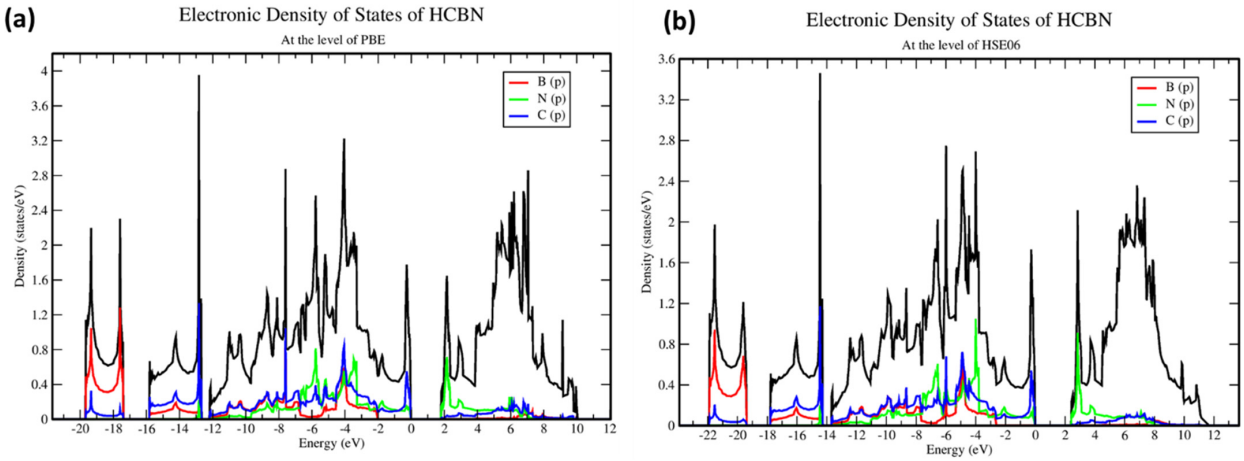

Figure 3. Electronic density of states (DOS) and partial density of states (PDOS) of HCBN calculated at the (**a**) PBE and (**b**) HSE06 levels.

3.2. Lattice Vibrations

A crystal with equilibrium lattice parameters is said to be dynamically stable if the potential energy increases with respect to any given set of atomic displacements. In the regime of the harmonic approximation, this corresponds to the real and positive phonon frequencies of all phonon modes. However, it is possible to have modes with negative or imaginary frequencies, which can be seen in the solution of an eigenvalue problem of the dynamical matrix [57]. If that occurs, it suggests dynamical instability of the crystal structure. In our previous study [16], we calculated phonon dispersions of h-BN and graphene and compared the results with previous studies. Our results are consistent with the existing theoretical and experimental reports. In the present study, we focused on the lattice dynamics of HCBN. Figure 4 shows the phonon dispersion of the primitive cell of HCBN. It can be seen that the dispersion relation has no imaginary frequency, which suggests that HCBN is dynamically stable. Since the primitive cell of HCBN is made up of four atoms, the phonon modes are described by 12 phonon branches, which include three acoustics and nine optical branches. Thus, the vibrational properties of HCBN are quite dissimilar to graphene and h-BN, which have a smaller number of planar modes. Nevertheless, there is a slight resemblance between the phonon dispersions of HCBN, graphene, and h-BN. Specifically, all three materials have linear longitudinal and transversal acoustic phonon branches, while the out-of-plane transversal acoustic (ZA) branch is quadratic in the neighborhood of q = 0, which is a peculiar characteristic of the phonon spectra of layered materials [58].

3.3. Thermodynamic Properties

The knowledge of LTECs of materials is very important; in particular, it is crucial for the epitaxial growths of crystals and can be linked to material properties such as the energy bandgap and consequently the optical properties. Moreover, LTEC is one of the quantities often considered in the design of high-speed integrated circuits for heat management. In this section, we present our results on the LTEC of HCBN using the QHA approximation and phonon dispersion at the LDA level. It was demonstrated that HCBN comprises carbon and boron nitride chains. Therefore, we first present the LTECs of pristine h-BN and graphene. This is necessary to validate our computational procedures by comparing our results to the thermodynamic properties of h-BN and graphene reported in other experimental [41] and theoretical [38,39] studies. Additionally, the computed properties of h-BN and graphene are compared with those of HCBN in order to assess the uniqueness of the LTEC of the hybrid material with respect to the parent systems.

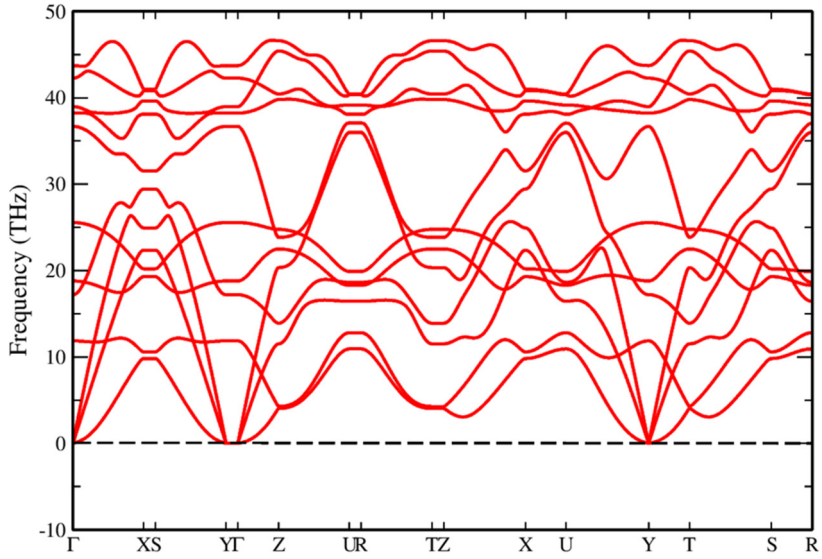

Figure 4. Phonon dispersion relation of HCBN calculated at the local density approximation (LDA) level.

Before presenting the thermal expansion properties, we first account for the effect of zero-point (ZP) motion. Figure 5 shows the energy vs. lattice constant curves for h-BN and graphene. The fitting of the data points was done using a cubic order polynomial. From the plots, we obtained 2.45 (Figure 5a) and 2.49 Å (Figure 5b) as the equilibrium lattice constants of graphene and h-BN, respectively. For graphene, the change in the lattice constant due to ZP energy was about +0.2% which is comparable to the value obtained as a result of temperature effects within 0 to 1000 K. For h-BN, the addition of zero-point energy changed the lattice parameter by +0.3%.

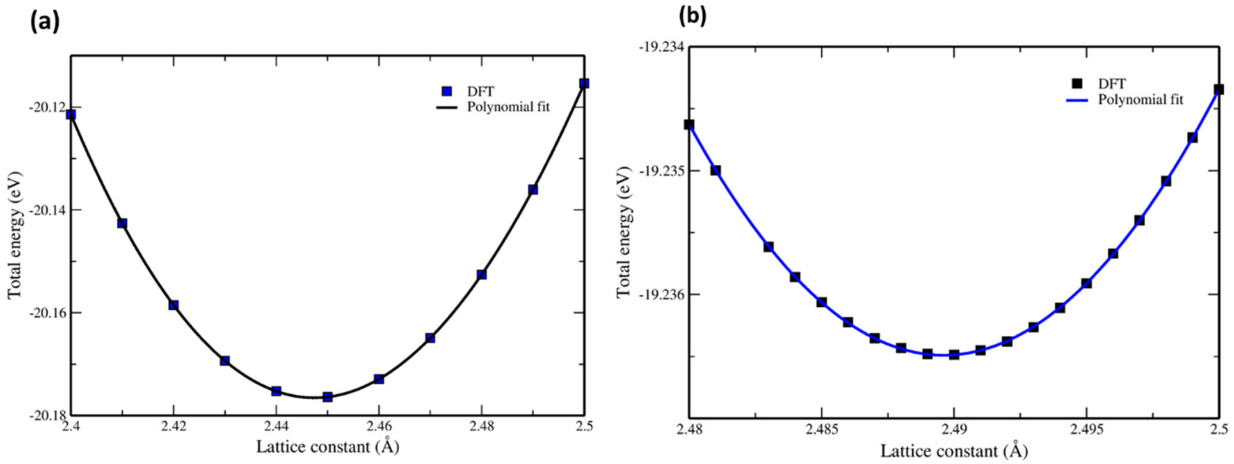

Figure 5. Optimized energy versus lattice constant curves of (**a**) graphene and (**b**) h-BN, calculated at the LDA level without zero-point energy. The smooth curves are polynomial fits, while the filled squares are total energies from DFT.

To investigate the LTEC within QHA, we performed a series of DFPT calculations by varying the lattice constant within the interval of ±0.5%. Generally, in 2D materials, the out-of-plane transversal acoustic mode is very soft, so the applied strain to the lattice must be considerably small. Otherwise, imaginary frequencies would be produced near the gamma point, which would invalidate QHA. In Figure 6, we present our calculated LTECs of h-BN and graphene along with the data from relevant earlier studies. From the graphs, it is seen that both h-BN and graphene have negative LTECs (or thermal contraction) of the same order, 10^{-6} K^{-1}, which are more prominent at low temperatures. The thermal

contraction over a broad spectrum of temperatures is more pronounced in h-BN than in graphene. In general, the temperature dependence of the LTEC for the two materials shows the same trend; it has a minimum within the interval of 0 to 300 K, beyond which it rises monotonically. These features of the LTEC curves can be explained, in line with Reference [59], as follows.

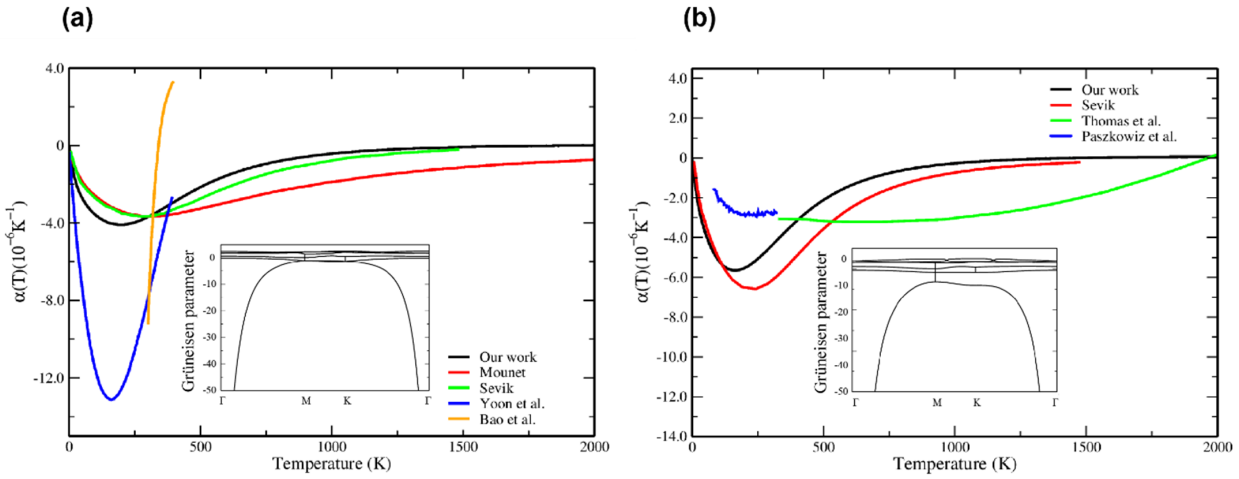

Figure 6. LTECs of (**a**) graphene, where the black color curve denotes our work, and other colors are for References [18,37, 41,42], and (**b**) h-BN where the black color curve denotes our work, and other colors are for References [60,61]. The insets are the mode-dependent Grüneisen parameters for the parent systems.

At low temperatures, the out-of-plane transversal acoustic (ZA) mode becomes populated and contributes more than the other modes to the negative Grüneisen parameter (see the insets in Figure 6a,b) and thus to the negative thermal expansions. The ZA mode dominates (see the insets in Figure 6) up to a certain temperature, after which the optical modes become excited and contribute to the positive Grüneisen parameter and consequently to the thermal expansion. As a result, the curves rise up. It is worth mentioning that the mode-dependent Grüneisen parameter describes contributions to the LTECs of crystals in terms of the modes of vibrations. Thus, a large negative Grüneisen parameter due to the ZA mode corresponds to large thermal contraction. Overall, our computed LTECs of h-BN and graphene agree, in terms of the order and features, with earlier theoretical [18,37,60] and experimental [41,42,61] studies but quantitatively differ, as shown in Figure 6. For graphene, our result is quite similar to the theoretical studies by Reference [18] (shown by the green curve in Figure 6a). The slight quantitative difference might be attributed to the difference between the computational parameters (such as the applied strain) for our study and theirs. With respect to the experimental results, even though they are widely dispersed, the deviation between the theoretical (including our result) and the experimental studies of Reference [41] (orange color curve) and [42] (blue color curve) might be associated with the limitations of QHA (such as the exclusion of anharmonicity) within DFPT or perturbation due to the substrate effect on graphene.

Following the computation of the LTECs of h-BN and graphene, which are consistent with other studies, we applied the same method to compute the LTEC of HCBN. Figure 7a shows the LTEC of HCBN in comparison with that of graphene and h-BN. As observed in h-BN and graphene, HCBN has negative LTECs but of smaller magnitude than the two parent materials. The thermal contraction occurs over a smaller range of temperature (0–300 K) than in the case of h-BN and graphene, for which it spans the range up to 1000 K. The LTEC curve of HCBN is quite unique; it decreases with temperature and reaches a minimum of -1.0×10^{-6} K^{-1} within 0 to 80 K, then it rises until a maximum of $+0.6 \times 10^{-6}$ K^{-1} is attained at around 500 K. Beyond this temperature, the LTEC steadily decreases with temperature and remains positive up to 1000 K. To further analyze the features of the curve, Figure 7b shows the in-plane mode-dependent Grüneisen parameter for HCBN. At low

temperature, when most of the optical modes are not excited, the lowest acoustic mode becomes excited, yielding the dominant negative Grüneisen parameter and contributing to the negative LTEC. As the temperature increases, the optical modes that correspond to the positive Grüneisen parameter become excited and contribute to the thermal expansion. It can be seen that the negative LTEC of HCBN due to the ZA mode is similar to that of the graphene and h-BN. This phenomenon is known as the "membrane effect" and was first proposed by Lifshitz [59] who suggested ZA (bending) modes in layered materials to be responsible for the negative LTECs. Recent studies [62–64] on thermal expansion of layered materials have confirmed this idea.

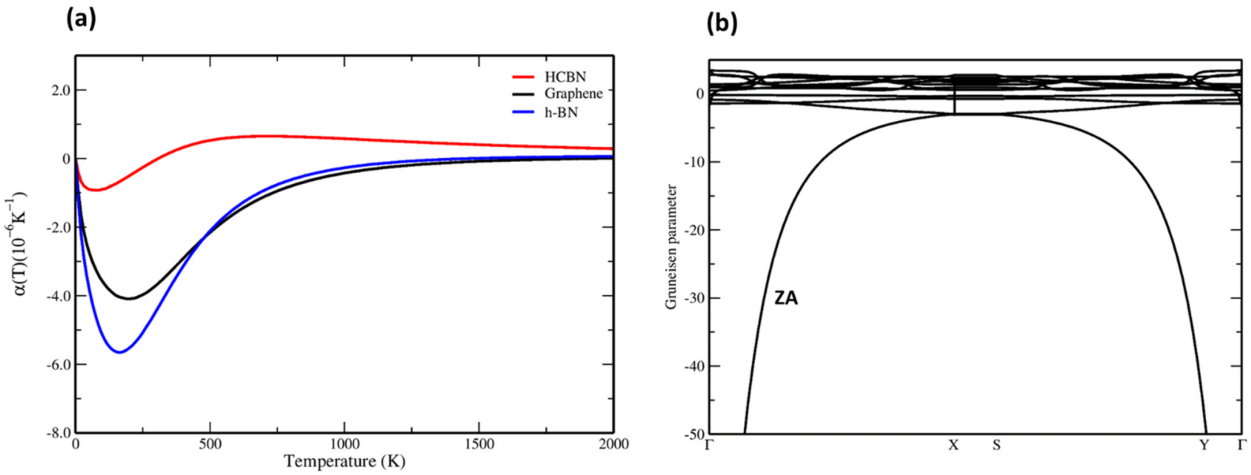

Figure 7. (**a**) LTECs for HCBN (red curve) compared with graphene (black curve) and h-BN (blue curve) (**b**) Grüneisen parameter for HCBN.

In the following, we present our results on other relevant thermodynamic properties, namely temperature-dependent heat capacities at constant pressure (C_p) and bulk moduli. Figure 8 shows the temperature-dependent specific heat capacities for all the three materials considered. The C_p was calculated using Equation (5), and it is nearly the same for all the three two-dimensional (2D) crystals, except at low and high temperatures. At room temperature, graphene has the lowest specific heat capacity, followed by HCBN, whereas the highest C_p was calculated for h-BN. However, at high temperatures around 1500 K, the order of the C_p is reversed. That is, graphene has the maximum value, followed by HCBN and h-BN. To validate our computational procedures for C_p, we compared our results with those of References [65,66] (the black circles and green triangles in Figure 8) and found a very good agreement with the literature values.

Finally, our results of the temperature-dependent isothermal bulk moduli for the three crystals are shown in Figure 9. From the figure, it is seen that the bulk moduli increase with the temperature for all the three systems considered in this study. Comparing the bulk modulus of HCBN with the parent systems at different temperatures, we observed that it is different except at certain temperatures. At 0 K, HCBN and graphene have the smallest and the largest bulk modulus, respectively. As the temperature increases, the bulk modulus of HCBN rises faster than for the parent systems, crossing the curves of h-BN and graphene bulk moduli at ~60 and 130 K, respectively. As the temperature increases to 300 K and beyond, HCBN attains the largest bulk modulus. Therefore, HCBN is the least compressible at high temperatures, while at 0 K it is the most compressible of the three considered 2D materials.

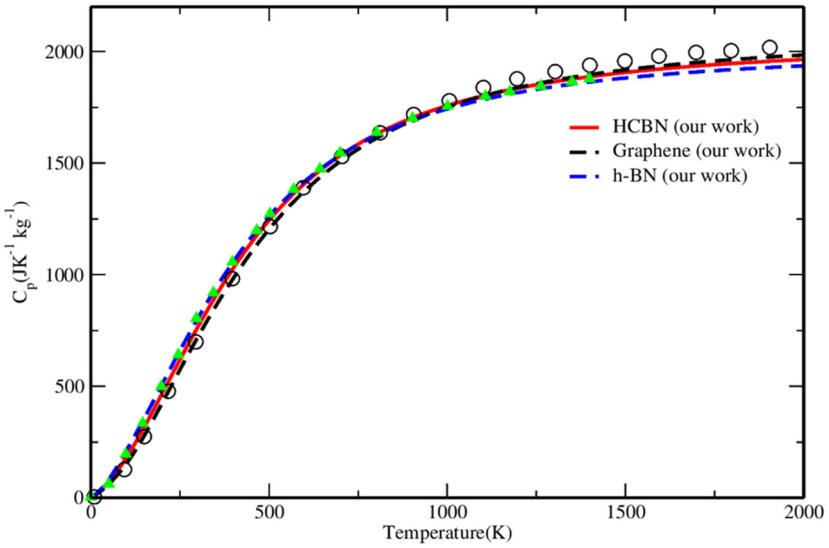

Figure 8. Specific heat capacities constant pressure (C_p) of graphene (black dashed curve), h-BN (blue dashed curve), and HCBN (red curve) compared with the results of Reference [65] (black circles) and [66] (green triangles).

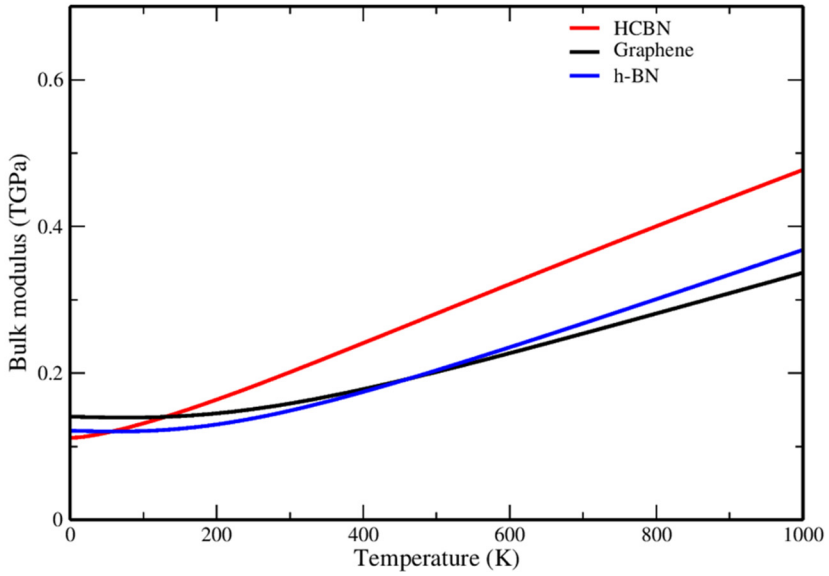

Figure 9. Temperature-dependent bulk moduli of HCBN (red curve), graphene (black curve), and h-BN (blue curve).

4. Conclusions

We present a first-principles study of the vibrational, electronic, and thermodynamic properties of HCBN and a comparison of the results with the corresponding properties of h-BN and graphene. The electronic properties were calculated at the HSE06 and PBE levels, while the vibrational and thermodynamic properties were computed at the level of LDA using QHA. All our calculated properties of h-BN and graphene are consistent with the available theoretical and experimental data from the literature.

Our calculations show that HCBN is a semiconductor with a finite bandgap of 2.43 eV. All positive frequencies of the phonon dispersion accede to its dynamic stability. The thermodynamic properties are as fascinating as those of graphene and h-BN. For instance, the C_p is comparable to the parent systems except at low and high temperatures. At low temperatures, the C_p is greater than that of graphene but lower than that of h-BN, while at

high temperatures, the C_p of HCBN is slightly greater than that of h-BN but lower than that of graphene. The rising response of the bulk modulus to changes in temperature is more rapid than for the parent systems. Compared to h-BN and graphene, HCBN is more compressible at low temperatures, whereas at high temperatures it is the least compressible of the three systems.

The membrane effect proposed by Lifshitz [59] and considered to be a characteristic of layered materials is also observed in HCBN; the negative thermal expansion is due to the main contribution from a ZA (out-of-plane acoustic) phonon mode. This mode leads to a largely negative Grüneisen parameter, the contribution of which to the negative LTEC dominates over other (planar) modes at low temperatures. However, at high temperatures, HCBN has a positive thermal expansion coefficient, while LTECs of the parent systems remain negative even up to 1000 K. HCBN has the smallest thermal contraction in comparison with the parent systems at low temperatures but a positive and finitely small LTEC at high temperatures. It is important to mention that 2D materials with high bulk moduli and low LTECs are sought after in ultra-fast integrated electronic devices for heat management. h-BN and graphene are known to be suitable for such applications. However, they are not suited for applications where semiconductors are required. The HCBN investigated in this study is a semiconductor and has a lower LTEC than the parent systems. Moreover, the bulk modulus is superior to the parent systems at high temperatures.

Author Contributions: Conceptualization, O.O.; methodology, O.O.; investigation, O.O.; resources, L.V.M.; writing—original draft preparation, O.O.; writing—review and editing, L.V.M.; supervision, L.V.M.; project administration, L.V.M. All authors have read and agreed to the published version of the manuscript.

Funding: This research received no external funding.

Institutional Review Board Statement: Not applicable.

Informed Consent Statement: Not applicable.

Data Availability Statement: The data that supports the findings of this study are available within the article.

Acknowledgments: The authors would like to acknowledge the support and resources from the Center for High Performance Computing (CHPC), South Africa.

Conflicts of Interest: The authors declare no conflict of interest.

References

1. Geim, A.K. Graphene: Status and prospects. *Science* **2009**, *324*, 1530–1534. [CrossRef] [PubMed]
2. Shi, Y.; Hamsen, C.; Jia, X.; Kim, K.K.; Reina, A.; Hofmann, M.; Hsu, A.L.; Zhang, K.; Li, H.; Juang, Z.Y.; et al. Synthesis of few-layer hexagonal boron nitride thin film by chemical vapor deposition. *Nano Lett.* **2010**, *10*, 4134–4139. [CrossRef] [PubMed]
3. Avouris, P. Graphene: Electronic and photonic properties and devices. *Nano Lett.* **2010**, *10*, 4285–4294. [CrossRef] [PubMed]
4. Golberg, D.; Bando, Y.; Huang, Y.; Terao, T.; Mitome, M.; Tang, C.; Zhi, C. Boron nitride nanotubes and nanosheets. *ACS Nano* **2010**, *4*, 2979–2993. [CrossRef]
5. Novoselov, K.S.; Geim, A.K.; Morozov, S.V.; Jiang, D.; Katsnelson, M.I.; Grigorieva, I.V.; Dubonos, S.V.; Firsov, A.A. Two-dimensional gas of massless Dirac fermions in graphene. *Nature* **2005**, *438*, 197–200. [CrossRef]
6. Zhang, Y.; Tan, Y.W.; Stormer, H.L.; Kim, P. Experimental observation of the quantum Hall effect and Berry's phase in graphene. *Nature* **2005**, *438*, 201–204. [CrossRef]
7. Neek-Amal, M.; Beheshtian, J.; Sadeghi, A.; Michel, K.H.; Peeters, F.M. Boron nitride monolayer: A strain-tunable nanosensor. *J. Phys. Chem. C* **2013**, *117*, 13261–13267. [CrossRef]
8. Radisavljevic, B.; Radenovic, A.; Brivio, J.; Giacometti, V.; Kis, A. Single-layer MoS_2 transistors. *Nat. Nanotechnol.* **2011**, *6*, 147–150. [CrossRef]
9. Tongay, S.; Zhou, J.; Ataca, C.; Liu, J.; Kang, J.S.; Matthews, T.S.; You, L.; Li, J.; Grossman, J.C.; Wu, J. Broad-range modulation of light emission in two-dimensional semiconductors by molecular physisorption gating. *Nano Lett.* **2013**, *13*, 2831–2836. [CrossRef]
10. Scarpa, F.; Adhikari, S.; Srikantha Phani, A. Effective elastic mechanical properties of single layer graphene sheets. *Nanotechnology* **2009**, *20*, 065709. [CrossRef]
11. Li, C.; Bando, Y.; Zhi, C.; Huang, Y.; Golberg, D. Thickness-dependent bending modulus of hexagonal boron nitride nanosheets. *Nanotechnology* **2009**, *20*, 385707. [CrossRef]

12. Serrano, J.; Bosak, A.; Arenal, R.; Krisch, M.; Watanabe, K.; Taniguchi, T.; Kanda, H.; Rubio, A.; Wirtz, L. Vibrational properties of hexagonal boron nitride: Inelastic X-ray scattering and Ab Initio calculations. *Phys. Rev. Lett.* **2007**, *98*, 095503. [CrossRef] [PubMed]
13. Seol, J.H.; Jo, I.; Moore, A.L.; Lindsay, L.; Aitken, Z.H.; Pettes, M.T.; Li, X.; Yao, Z.; Huang, R.; Broido, D.; et al. Two-dimensional phonon transport in supported graphene. *Science* **2010**, *328*, 213–216. [CrossRef] [PubMed]
14. Balandin, A.A.; Ghosh, S.; Bao, W.; Calizo, I.; Teweldebrhan, D.; Miao, F.; Lau, C.N. Superior thermal conductivity of single-layer graphene. *Nano Lett.* **2008**, *8*, 902–907. [CrossRef] [PubMed]
15. Singh, S.K.; Neek-Amal, M.; Costamagna, S.; Peeters, F.M. Thermomechanical properties of a single hexagonal boron nitride sheet. *Phys. Rev. B Condens. Matter Mater. Phys.* **2013**, *87*, 184106. [CrossRef]
16. Olaniyan, O.; Moskaleva, L.; Mahadi, R.; Igumbor, E.; Bello, A. Tuning the electronic structure and thermodynamic properties of hybrid graphene-hexagonal boron nitride monolayer. *FlatChem* **2020**, *24*, 100194. [CrossRef]
17. Olaniyan, O.; Maphasha, R.E.; Madito, M.J.; Khaleed, A.A.; Igumbor, E.; Manyala, N. A systematic study of the stability, electronic and optical properties of beryllium and nitrogen co-doped graphene. *Carbon N. Y.* **2018**, *129*, 207–227. [CrossRef]
18. Sevik, C. Assessment on lattice thermal properties of two-dimensional honeycomb structures: Graphene, h-BN, h-MoS_2, and h-$MoSe_2$. *Phys. Rev. B Condens. Matter Mater. Phys.* **2014**, *89*, 035422. [CrossRef]
19. Lau, K.C.; Pandey, R. Thermodynamic stability of novel boron sheet configurations. *J. Phys. Chem. B* **2008**, *112*, 10217–10220. [CrossRef]
20. Kouvetakis, J.; Kaner, R.B.; Sattler, M.L.; Bartlett, N. A novel graphite-like material of composition BC_3, and nitrogen-carbon graphites. *J. Chem. Soc. Chem. Commun.* **1986**, *24*, 1758–1759. [CrossRef]
21. Lowther, J.E.; Zinin, P.V.; Ming, L.C. Vibrational energies of graphene and hexagonal structured planar B-C complexes. *Phys. Rev. B Condens. Matter Mater. Phys.* **2009**, *79*, 033401. [CrossRef]
22. Hu, Q.; Wu, Q.; Ma, Y.; Zhang, L.; Liu, Z.; He, J.; Sun, H.; Wang, H.T.; Tian, Y. First-principles studies of structural and electronic properties of hexagonal BC_5. *Phys. Rev. B Condens. Matter Mater. Phys.* **2006**, *73*, 214116. [CrossRef]
23. Zhou, Y.; Wang, Z.; Yang, P.; Gao, F. Novel electronic and magnetic properties of graphene nanoflakes in a boron nitride layer. *J. Phys. Chem. C* **2012**, *116*, 7581–7586. [CrossRef]
24. Kan, M.; Zhou, J.; Wang, Q.; Sun, Q.; Jena, P. Tuning the band gap and magnetic properties of BN sheets impregnated with graphene flakes. *Phys. Rev. B Condens. Matter Mater. Phys.* **2011**, *84*, 205412. [CrossRef]
25. Ci, L.; Song, L.; Jin, C.; Jariwala, D.; Wu, D.; Li, Y.; Srivastava, A.; Wang, Z.F.; Storr, K.; Balicas, L.; et al. Atomic layers of hybridized boron nitride and graphene domains. *Nat. Mater.* **2010**, *9*, 430–435. [CrossRef]
26. Suenaga, K.; Colliex, C.; Demoncy, N.; Loiseau, A.; Pascard, H.; Willaime, F. Synthesis of nanoparticles and nanotubes with well-separated layers of boron nitride and carbon. *Science* **1997**, *278*, 653–655. [CrossRef]
27. Han, W.Q.; Mickelson, W.; Cumings, J.; Zettl, A. Transformation of $B_xC_yN_z$ nanotubes to pure BN nanotubes. *Appl. Phys. Lett.* **2002**, *81*, 1110–1112. [CrossRef]
28. Kawasaki, T.; Ichimura, T.; Kishimoto, H.; Akbar, A.A.; Ogawa, T.; Oshima, C. Double atomic layers of graphene/monolayer h-BN on Ni(111) studied by scanning tunneling microscopy and scanning tunneling spectroscopy. *Surf. Rev. Lett.* **2002**, *9*, 1459–1464. [CrossRef]
29. Giovannetti, G.; Khomyakov, P.A.; Brocks, G.; Kelly, P.J.; van den Brink, J. Substrate-induced band gap in graphene on hexagonal boron nitride: Ab initio density functional calculations. *Phys. Rev. B* **2007**, *76*, 073103. [CrossRef]
30. Pruneda, J.M. Origin of half-semimetallicity induced at interfaces of C-BN heterostructures. *Phys. Rev. B Condens. Matter Mater. Phys.* **2010**, *81*, 161409. [CrossRef]
31. Fan, X.; Shen, Z.; Liu, A.Q.; Kuo, J.L. Band gap opening of graphene by doping small boron nitride domains. *Nanoscale* **2012**, *4*, 2157–2165. [CrossRef]
32. Jung, J.; Qiao, Z.; Niu, Q.; MacDonald, A.H. Transport properties of graphene nanoroads in boron nitride sheets. *Nano Lett.* **2012**, *12*, 2936–2940. [CrossRef]
33. Wu, M.M.; Zhong, X.; Wang, Q.; Sun, Q.; Pandey, R.; Jena, P. Anisotropy and transport properties of tubular C-BN Janus nanostructures. *J. Phys. Chem. C* **2011**, *115*, 23978–23983. [CrossRef]
34. Bernardi, M.; Palummo, M.; Grossman, J.C. Optoelectronic properties in monolayers of hybridized graphene and hexagonal boron nitride. *Phys. Rev. Lett.* **2012**, *108*, 226805. [CrossRef]
35. Ge, M.; Si, C. Mechanical and electronic properties of lateral graphene and hexagonal boron nitride heterostructures. *Carbon N. Y.* **2018**, *136*, 286–291. [CrossRef]
36. Pavone, P.; Karch, K.; Schütt, O.; Strauch, D.; Windl, W.; Giannozzi, P.; Baroni, S. Ab initio lattice dynamics of diamond. *Phys. Rev. B* **1993**, *48*, 3156–3163. [CrossRef]
37. Mounet, N.; Marzari, N. First-principles determination of the structural, vibrational and thermodynamic properties of diamond, graphite, and derivatives. *Phys. Rev. B Condens. Matter Mater. Phys.* **2005**, *71*, 1–14. [CrossRef]
38. Zakharchenko, K.V.; Katsnelson, M.I.; Fasolino, A. Finite temperature lattice properties of graphene beyond the quasiharmonic approximation. *Phys. Rev. Lett.* **2009**, *102*, 046808. [CrossRef]
39. Zakharchenko, K.V.; Los, J.H.; Katsnelson, M.I.; Fasolino, A. Atomistic simulations of structural and thermodynamic properties of bilayer graphene. *Phys. Rev. B Condens. Matter Mater. Phys.* **2010**, *81*, 235439. [CrossRef]

40. Los, J.H.; Ghiringhelli, L.M.; Meijer, E.J.; Fasolino, A. Improved long-range reactive bond-order potential for carbon. I. Construction. *Phys. Rev. B Condens. Matter Mater. Phys.* **2005**, *72*, 214102. [CrossRef]
41. Bao, W.; Miao, F.; Chen, Z.; Zhang, H.; Jang, W.; Dames, C.; Lau, C.N. Controlled ripple texturing of suspended graphene and ultrathin graphite membranes. *Nat. Nanotechnol.* **2009**, *4*, 562–566. [CrossRef] [PubMed]
42. Yoon, D.; Son, Y.W.; Cheong, H. Negative thermal expansion coefficient of graphene measured by raman spectroscopy. *Nano Lett.* **2011**, *11*, 3227–3231. [CrossRef] [PubMed]
43. Kresse, G.; Hafner, J. Ab initio molecular dynamics for liquid metals. *Phys. Rev. B* **1993**, *47*, 558–561. [CrossRef] [PubMed]
44. Kresse, G.; Furthmüller, J. Efficient iterative schemes for ab initio total-energy calculations using a plane-wave basis set. *Phys. Rev. B Condens. Matter Mater. Phys.* **1996**, *54*, 11169–11186. [CrossRef] [PubMed]
45. Joubert, D. From ultrasoft pseudopotentials to the projector augmented-wave method. *Phys. Rev. B Condens. Matter Mater. Phys.* **1999**, *59*, 1758–1775.
46. Hedin, L.; Lundqvist, B.I. Explicit local exchange-correlation potentials. *J. Phys. C Solid State Phys.* **1971**, *4*, 2064–2083. [CrossRef]
47. Perdew, J.P.; Burke, K.; Ernzerhof, M. Generalized gradient approximation made simple. *Phys. Rev. Lett.* **1996**, *77*, 3865–3868. [CrossRef]
48. Heyd, J.; Scuseria, G.E. Efficient hybrid density functional calculations in solids: Assessment of the Heyd-Scuseria-Ernzerhof screened Coulomb hybrid functional. *J. Chem. Phys.* **2004**, *121*, 1187–1192. [CrossRef]
49. Monkhorst, H.J.; Pack, J.D. Special points for Brillouin-zone integrations. *Phys. Rev. B* **1976**, *13*, 5188–5192. [CrossRef]
50. Maradudin, A.; Montroll, E.; Weiss, G.; Ipatova, I. *Theory of Lattice Dynamics in the Harmonic Approximation*, 2nd ed.; Academic Press: New York, NY, USA, 1971.
51. Geim, A.K.; Novoselov, K.S. The rise of graphene. *Nat. Mater.* **2007**, *6*, 183–191. [CrossRef]
52. Cassabois, G.; Valvin, P.; Gil, B. Hexagonal boron nitride is an indirect bandgap semiconductor. *Nat. Photonics* **2016**, *10*, 262–266. [CrossRef]
53. Reina, A.; Jia, X.; Ho, J.; Nezich, D.; Son, H.; Bulovic, V.; Dresselhaus, M.S.; Jing, K. Large area, few-layer graphene films on arbitrary substrates by chemical vapor deposition. *Nano Lett.* **2009**, *9*, 30–35. [CrossRef] [PubMed]
54. Li, X.; Cai, W.; An, J.; Kim, S.; Nah, J.; Yang, D.; Piner, R.; Velamakanni, A.; Jung, I.; Tutuc, E.; et al. Large-area synthesis of high-quality and uniform graphene films on copper foils. *Science* **2009**, *324*, 1312–1314. [CrossRef] [PubMed]
55. Preobrajenski, A.B.; Vinogradov, A.S.; Mårtensson, N. Monolayer of h-BN chemisorbed on Cu(111) and Ni(111): The role of the transition metal 3d states. *Surf. Sci.* **2005**, *582*, 21–30. [CrossRef]
56. Li, X.; Cai, W.; Colombo, L.; Ruoff, R.S. Evolution of graphene growth on Ni and Cu by carbon isotope labeling. *Nano Lett.* **2009**, *9*, 4268–4272. [CrossRef]
57. Togo, A.; Tanaka, I. First principles phonon calculations in materials science. *Scr. Mater.* **2015**, *108*, 1–5. [CrossRef]
58. Zabel, H. Phonons in layered compounds. *J. Phys. Condens. Matter* **2001**, *13*, 7679–7690. [CrossRef]
59. Lifshitz, I. Thermal properties of chain and layered structures at low temperatures. *Zh. Eksp. Teor. Fiz* **1952**, *22*, 475–486.
60. Thomas, S.; Ajith, K.M.; Chandra, S.; Valsakumar, M.C. Temperature dependent structural properties and bending rigidity of pristine and defective hexagonal boron nitride. *J. Phys. Condens. Matter* **2015**, *27*, 315302. [CrossRef]
61. Paszkowicz, W.; Pelka, J.B.; Knapp, M.; Szyszko, T.; Podsiadlo, S. Lattice parameters and anisotropic thermal expansion of hexagonal boron nitride in the 10-297.5 K temperature range. *Appl. Phys. A Mater. Sci. Process.* **2002**, *75*, 431–435. [CrossRef]
62. Belenkii, G.L.; Suleimanov, R.A.; Abdullaev, N.A.; Shteinshraiber, V.Y. Thermal expansion of layered crystals. Lifshits Models. *Fiz. Tverd. Tela* **1984**, *26*, 3560–3566.
63. Abdullaev, N.A. Grüneisen parameters for layered crystals. *Phys. Solid State* **2001**, *43*, 727–731. [CrossRef]
64. Abdullaev, N.A.; Suleimanov, R.A.; Aldzhanov, M.A.; Alieva, L.N. On the role played by bending vibrations in heat transfer in layered crystals. *Phys. Solid State* **2002**, *44*, 1859–1863. [CrossRef]
65. Tohei, T.; Kuwabara, A.; Oba, F.; Tanaka, I. Debye temperature and stiffness of carbon and boron nitride polymorphs from first principles calculations. *Phys. Rev. B Condens. Matter Mater. Phys.* **2006**, *73*, 063304. [CrossRef]
66. Hultgren, R.; Desai, P.; Hawkins, D.; Gleiser, M.; Kelley, K. *Selected Values of the Thermodynamic Properties of the Elements*; American Society for Metals: Metals Park, OH, USA, 1973.